Nanoscale Electron Bunching in Laser-Triggered Ionization Injection in Plasma Accelerators

X. L. Xu,[1] C.-H. Pai,[2] C. J. Zhang,[2] F. Li,[2] Y. Wan,[2] Y. P. Wu,[2] J. F. Hua,[2] W. Lu,[2,3,*] W. An,[1] P. Yu,[1] C. Joshi,[1] and W. B. Mori[1]
[1]*University of California, Los Angeles, California 90095, USA*
[2]*Department of Engineering Physics, Tsinghua University, Beijing 100084, China*
[3]*IFSA Collaborative Innovation Center, Shanghai Jiao Tong University, Shanghai 200240, China*
(Received 7 October 2015; published 15 July 2016)

Ionization injection is attractive as a controllable injection scheme for generating high quality electron beams using plasma-based wakefield acceleration. Because of the phase-dependent tunneling ionization rate and the trapping dynamics within a nonlinear wake, the discrete injection of electrons within the wake is nonlinearly mapped to a discrete final phase space structure of the beam at the location where the electrons are trapped. This phenomenon is theoretically analyzed and examined by three-dimensional particle-in-cell simulations which show that three-dimensional effects limit the wave number of the modulation to between $> 2k_0$ and about $5k_0$, where k_0 is the wave number of the injection laser. Such a nanoscale bunched beam can be diagnosed by and used to generate coherent transition radiation and may find use in generating high-power ultraviolet radiation upon passage through a resonant undulator.

DOI: 10.1103/PhysRevLett.117.034801

Because of the ability to sustain ultrahigh acceleration gradients (GV/cm), the field of plasma-based wakefield acceleration has attracted much attention in the past two decades [1]. Recently, ionization injection has been proposed and demonstrated [2–9] as a viable injection scheme and investigated for generating high brightness ($\sim 10^{19}$ A/rad^2/m^2), stable, and tunable electron beams [10–15]. The basic idea is that the trapping threshold of an electron is reduced when it is born inside the wakefield near the maximum of the wake's potential compared to an electron from a preionized plasma. Such high brightness beams are needed for future free-electron-laser (FEL) and collider applications.

The key to generating a high brightness beam is to limit the volume within the wake where the injection of electrons occurs [16]. In the case where the injection is from field ionization due to a laser pulse, the ionization volume is limited by choosing the intensity of the injection pulse(s) close the ionization threshold of the bound electrons. Therefore, electrons are mostly born near the peaks and the troughs of the oscillating laser electric field. The phase-dependent ionization leads to an intrinsic initial phase space discretization at twice the optical frequency, which is known to produce third harmonic generation in tunnel ionized plasma [17,18].

We show in this Letter using theory and fully three-dimensional (3D) particle-in-cell (PIC) simulations that when ionization occurs on either side of the peak of the wake potential, the electron bunch can be strongly modulated in space on the nanometer scale when it becomes trapped. In the 1D limit, the spacing of the modulations can be made arbitrarily small. However, we show that 3D effects limit the discretization pattern to less than one-fifth the laser wavelength. In previous work, the generation of distinct energy peaks within a single bunch were described from ionization in different optical cycles [19] or from ionization at distinct propagation times [20]. On the other hand, here we show that ionization injection within each optical phase of the laser at one propagation distance can lead to the formation of distinct current peaks. Such an ultrashort and nanobunched electron beam can be diagnosed by and used to generate coherent transition radiation (CTR) [21], could generate a train of attosecond x-ray pulses through betatron radiation in the plasma wake, and be used to produce high-power coherent EUV radiation in a short resonant undulator.

To illustrate the concept, we first consider ionization injection using a single laser pulse as shown in Fig. 1(a). An 800 nm laser pulse polarized in the x direction with normalized vector potential $a_0 = 2$, $w_0 = 14\ \mu$m, and a pulse length (FWHM of energy) of 26 fs, propagates into a mixture of preionized plasma ($n_p = 2 \times 10^{18}$ cm^{-3}) and N^{5+} ions. The preionized electrons form a nonlinear wake. As has been observed previously [4], the K-shell electrons of nitrogen with high ionization potentials (IPs) are released during the rising edge of the wake potential [Fig. 1(a)], then slip to the back of the wake where some of these electrons are trapped [4]. This process is examined using the 3D PIC code OSIRIS [22] using a moving window [23]. We define the z axis to be the laser propagating direction. The code uses the Ammosov-Delone-Krainov (ADK) tunneling ionization model [24]. The IPs of the sixth and seventh nitrogen electrons are $I_p \approx 552.1$ and 667.0 eV, respectively, and the Keldysh parameter in this

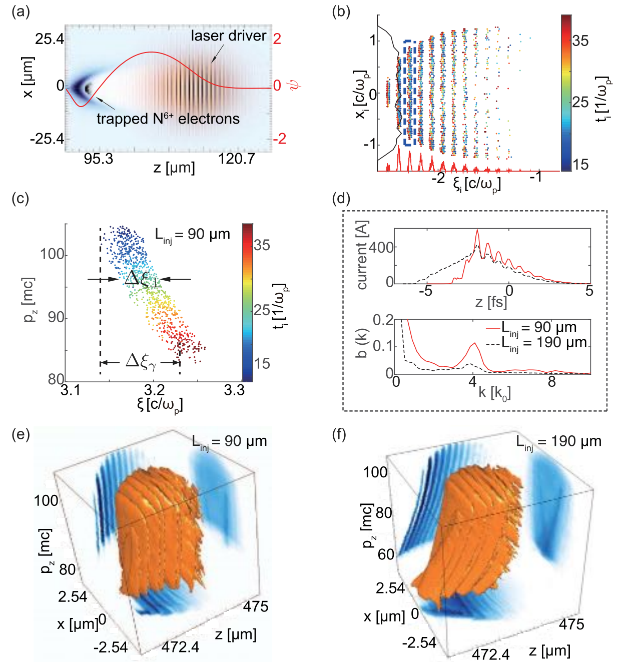

FIG. 1. The nanoscale bunching of injected charge in a laser-driven plasma accelerator. The laser is focused at the $z = 0$ mm plane. (a) Snapshot of the charge density distribution of the background electrons, the K-shell electrons of nitrogen, and the laser electric field in the x direction. The red line is the on-axis pseudopotential ψ. (b) The distribution of the ionization injected electrons in (ξ_i, x_i) space. The color represents the time when the electrons are ionized. The red peaks are integrated injected charge in x_i, whereas the black is the integrated injected charge for all ξ_i. (c) The (ξ, p_z) space at $z = 0.5$ mm for an initial slice indicated by the dashed box in (b). (d) The current profile and the bunching factor at $z = 0.5$ mm. (e),(f) show the (z, x, p_z) phase space at $z = 0.5$ mm. For the $L_{\rm inj} = 90\ \mu$m case, the N^{5+} ions are distributed from $z = 0.038$ to 0.128 mm and $n_{N^{5+}} = 10^{-3} n_p$; for the $L_{\rm inj} = 190\ \mu$m case, the N^{5+} ions are distributed from $z = 0.038$ to 0.228 mm and $n_{N^{5+}} = 5 \times 10^{-4} n_p$.

simulation is $\gamma_K = \sqrt{I_p/2U_p} \approx 0.023,\ 0.021 \ll 1$; therefore, the ADK model should be valid. The simulation window has a dimension of $63.5 \times 63.5 \times 38.1\ \mu$m with $500 \times 500 \times 1500$ cells in the x, y, and z directions, respectively.

The (ξ_i, x_i) space distribution of the trapped electrons when they are ionized is shown in Fig. 1(b), where $\xi \equiv v_\phi t - z$ is the relative longitudinal position, and v_ϕ is the phase velocity of the wake. Because of the laser phase-dependent ionization probability, the initial electron distribution has a strong modulation at $2k_0$, where k_0 is the wave number of the laser pulse. After being released, the electrons slip to the back of the wake and are accelerated by the longitudinal electric field in the wake. Under the quasistatic approximation, $\gamma - (v_\phi/c)p_z - \psi =$ const [25], where $\psi \equiv (e/mc^2)[\phi - (v_\phi/c)A_z]$ is the pseudopotential, ψ in the fully blown-out wake can be expressed as $\psi \approx [r_b^2(\xi) - r^2]/4$ [26,27]. Here, $r_b(\xi)$ is the normalized radius of the ion channel that has a spherical shape for a sufficiently large maximum blowout radius r_m given by $r_b^2(\xi) = r_m^2 - \xi^2$ [26,27]. Note that all parameters with units of length are normalized to the background plasma skin depth c/ω_p, where ω_p is the background plasma frequency. Using the constant of motion given above, the relative longitudinal position of the injected electron can be expressed as

$$\xi \approx \sqrt{4 + \xi_i^2 + r_i^2 - r^2 - 4[\gamma - (v_\phi/c)p_z]}, \qquad (1)$$

where subscript i refers to the position when the electrons are ionized. The electron conducts betatron oscillations in x and y with a decreasing amplitude under the focusing and acceleration fields [16,28]. An initial isolated slice in (ξ_i, x_i, y_i) will be mapped to an isolated slice in (ξ, x, y, p_z) space. If $r_i \ll 1$ and the transverse momentum (the vector potential of the laser at the time of ionization) are small, the electrons are relativistic, and $p_z/\gamma_\phi^2 \ll 2$ [i.e., $\gamma - (v_\phi/c)p_z \ll 1$], the position ξ is mainly determined by the initial ξ_i as $\xi \approx \sqrt{4 + \xi_i^2}$, which means the initial modulation in ξ_i can be nonlinearly mapped to ξ. This means that an initial slice will be mapped to the same final slice.

Any spread in r_i, r, and $\gamma - (v_\phi/c)p_z$ will broaden the ξ distribution for an initial slice. In Fig. 1(c), we show the (ξ, p_z) space at $z = 0.5$ mm for an initial slice [indicated by the dashed box in Fig. 1(b)]. One can see that the spread of ξ due to the spread of transverse motion is $\Delta\xi_\perp \approx 0.05$. For this example where a laser driver with moderate a_0 is used, we find that $1 - v_\phi/c \approx \omega_p^2/(2\omega_0^2)$ [29]. Therefore, the term $\gamma - (v_\phi/c)p_z \approx \gamma(1 - v_\phi/c) \approx \omega_p^2/(2\omega_0^2)\gamma$ contributes differently for electrons with different energy leading to a spread in ξ for electrons with the same ξ_i. Specifically, electrons ionized earlier (at different z_i) but at the same ξ_i can have higher energy and smaller ξ. In Fig. 1(c), the difference in ξ due to the energy difference is seen to be $\Delta\xi_\gamma \approx 0.1$. This spread depends on the spread in z_i which can be controlled by limiting the distance of ionization, $L_{\rm inj}$. In the simulations, we increased $L_{\rm inj}$ from 90 to 190 μm by varying the region where N^{5+} existed. In Figs. 1(d)–1(f), it can be seen that the difference of ξ due to this spread in energy is increased to $\Delta\xi_\gamma \approx 0.2$. The current profile and the bunching factor [defined as $b(k) = |\int dz g(z) \exp(ikz)|$, where $g(z)$ is the normalized distribution of the trapped electrons] are shown in Fig. 1(d). The modulation in the current profile is peaked at $k \approx 4k_0$, and the modulation and the bunching factor are reduced when $L_{\rm inj}$ is increased from 90 to 190 μm due to the larger $\Delta\xi_\gamma$. The discretized phase space structure can be seen clearly in (z, x, p_z) phase space at $z = 0.5$ mm as shown in Figs. 1(e) and 1(f); however, for the larger $L_{\rm inj}$, the slices are slanted in (p_z, z) space, indicating that within a narrow energy slice of the beam the bunching factor can still be large.

By using two pulses to separate the wake formation and the electron injection, the initial and final phase space of the trapped electrons can be better controlled [10,11,13–16]. Throughout the rest of this Letter, we consider the driver pulse to be a relativistic electron bunch and the injection pulse to be a copropagating low intensity laser pulse. The injection laser can be focused to a very small spot size to decrease the transverse ionization region, and due to its shorter Rayleigh length, it will have a shorter L_{inj}. This leads to a much reduced $\Delta\xi_\perp$ and $\Delta\xi_\gamma$. In a relativistic beam driver case, the phase velocity of the nonlinear wake is equal to the velocity of the driver bunch, which is typically closer to the speed of light than the group velocity of the laser. Therefore, the term $\Delta\xi_\gamma$ is much reduced. The electron is longitudinally frozen in the wake after it is boosted to relativistic energy. This longitudinal position can, therefore, be defined as ξ_f, and this is insensitive when it is ionized.

Under the assumption of no phase slippage in the wake, the effect of the nonlinear mapping between ξ_i and ξ_f and the finite r_i on the bunching factor can be quantified as follows. The distribution function of the final position within the wake, ξ_f, is $g(\xi_f)d\xi_f = d\xi_i \int dr_i f(r_i,\xi_i)$ which can be obtained from the distribution of the initial parameters $f(\xi_i, r_i)$, where r_f is neglected, which is reasonable when the energy of the electron is high. The bunching factor is $b(k) = |\int d\xi_i dr_i \exp(ik\xi_f) f(\xi_i, r_i)|$. Assuming $\delta\xi_i \equiv \xi_i - \bar{\xi}_i \ll \bar{\xi}_i$ and $r_i \ll \bar{\xi}_i$ where $\bar{\xi}_i$ is the mean value of ξ_i, then after expanding ξ_f to the order of $O(r_i^2)$ and $O(\delta\xi_i^2)$, ξ_f can be expressed as $\xi_f \approx \sqrt{4+\bar{\xi}_i^2}\{1+(\delta\xi_i/h_m^2\bar{\xi}_i) + (\delta\xi_i^2/2h_m^2\bar{\xi}_i^2)[1-(1/h_m^2)] + (r_i^2/2h_m^2\bar{\xi}_i^2)\}$, where $h_m = \sqrt{4+\bar{\xi}_i^2}/\bar{\xi}_i$ is the wave number upshift factor obtained from the nonlinear mapping process. We assume the initial distribution is $f(\xi_i, r_i) = (r_i/\sigma_r^2)\exp[-(r_i^2/2\sigma_r^2)] \times (1/\sqrt{2\pi}\sigma_e)\exp[-(\delta\xi_i^2/2\sigma_e^2)]\sum_{n=-\infty}^{+\infty} F_n \exp(-i2nk_0\delta\xi_i)$, where $F_n = \int d\xi_i f_b(\xi_i)\exp(i2nk_0\delta\xi_i)$ and $f_b(\xi_i)$ is the initial ξ_i distribution in a single slice. By substituting the expression of $f(\xi_i, r_i)$ into the bunching factor, it is straightforward to obtain

$$b(k) = \sum_{n=-\infty}^{+\infty} |F_n| R(\hat{\sigma}_r, \hat{\sigma}_e) e^{-\{[(k-2nh_m k_0)^2\sigma_e^2]/[2h_m^2(1+\hat{\sigma}_e^4)]\}}, \quad (2)$$

where $R(\hat{\sigma}_r, \hat{\sigma}_e) = [(1+\hat{\sigma}_r^4)(1+\hat{\sigma}_e^4)]^{-1/4}$ is the 3D reduction factor, $\hat{\sigma}_e = \sigma_e\sqrt{(1-1/h_m^2)k/(h_m\bar{\xi}_i)}$, and $\hat{\sigma}_r = \sigma_r\sqrt{k/(h_m\bar{\xi}_i)}$. The ratio of the strongest modulation wave number in the current profile over the wave number of the injection laser (the modulation factor) is

$$h = 2h_m = 2\sqrt{4+\bar{\xi}_i^2}/|\bar{\xi}_i|, \quad (3)$$

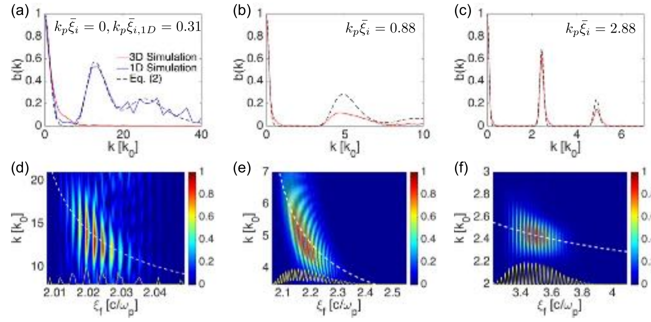

FIG. 2. Bunching of electrons when charges are injected by using a relatively low intensity laser pulse in a prescribed and nonevolving wakefield. (a)–(c) The red lines are the bunching factor while scanning the initial $\bar{\xi}_i$, and the dashed lines are the analytical results from Eq. (2). (d)–(f) The corresponding Wigner transform of the current profile showing the spatial modulation. The white dashed lines are $k/k_0 = 2\sqrt{4+\xi_i^2}/\xi_i$ and the yellow lines are the current profile of the injected charge. Note that (d) is a 1D simulation, and the others are 3D simulations.

where the factor 2 is from the ionization process, and the factor h_m is from the nonlinear mapping process. Equation (3) shows that the wavelength of the modulation is shortest for $\bar{\xi}_i$ near zero. However, $\hat{\sigma}_r$ becomes very large for $\bar{\xi}_i$ near zero; therefore, R will be small in this limit. For this reason, the wave number of the modulation is limited, and the modulation is only seen when ionization occurs off the maximum of the potential.

These conclusions are verified numerically. We use OSIRIS with nonevolving forces from the nonlinear wakefields, i.e., $F_z = -\xi/2$, $F_r = r/2 + (1-v_z)r/2$, so no background plasma electrons are needed. An 800 nm laser with $a_0 = 0.12$, $w_0 = 2\ \mu$m propagates through a plasma with $n_p = 1.74\times10^{17}\ \mathrm{cm}^{-3}$ and a $10^{-5}n_p$ He^{1+} plasma (to minimize space charge effects) provides the self-trapped electrons via laser ionization. The longitudinal delay between the laser pulse and the plane with $\xi = 0$ is scanned to generate electrons with different $\bar{\xi}_i$, and the resulting bunching factors are shown in Figs. 2(a)–2(c). When the laser is strongly focused, $\gamma - p_z - \psi$ is not strictly conserved, and the variation leads to a reduction of the bunching factor, which is more serious when h is larger [see Fig. 2(b)]. Because of the nonlinear mapping process, the modulation factor depends on ξ_f, which can be seen from the Wigner transform of the current profile as shown in Figs. 2(d)–2(f). The modulation factor can be very high theoretically when $\bar{\xi}_i$ is very close to zero, but in this case, R is very small so b is rather small. However, in a 1D simulation, h as high as 15 was observed, as shown in Fig. 2(d). In each simulation, the energy of the electrons is more than 100 MeV.

To verify that nanobunching exists at high energies including evolving wakes during trapping and acceleration, we next present results from a fully self-consistent 3D OSIRIS simulation. We use a relativistic electron beam to

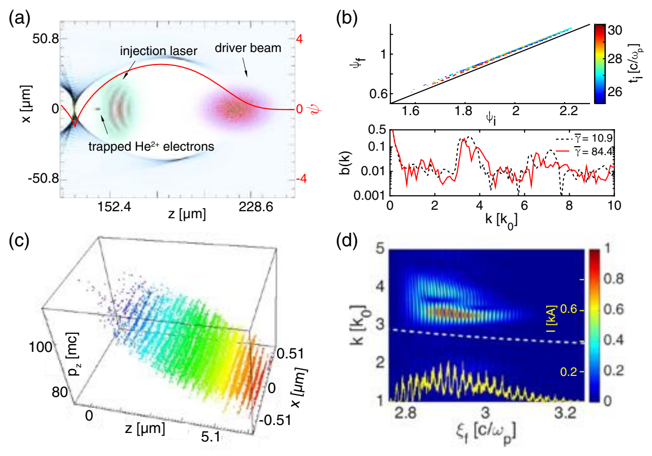

FIG. 3. An electron driver beam followed by an injection laser propagate to the right in a mixture of preionized plasma and He^{1+} ions ($n_p = 1.74 \times 10^{17}\ \mathrm{cm}^{-3}$, $n_{He^{1+}} = 0.1 n_p$). Driver beam: $E_b = 1$ GeV, $\sigma_r = 8.9\mu$m, $\sigma_z = 10.6\mu$m, $I_b = 19$ kA. The injection laser is the same as in the case of Fig. 2. (a) Snapshot of the charge density distribution of the background electrons, the second electron of helium, and the laser electric field. The red line is the pseudopotential at the center. (b) The dependence of the final ψ_f on the initial ψ_i for injected electrons and the bunching factor at $z = 0.1$ mm and $z = 0.9$ mm. The color represents the ionization time. The black line represents $\psi_f = \psi_i - 1$. (c) The (z, x, p_z) phase space distribution of the trapped electrons at $z = 0.9$ mm. The color represents the z position. (d) The current (yellow line) and the corresponding Wigner transform at $z = 0.9$ mm. The white line is $k/k_0 = 2\sqrt{4 + \xi_i^2}/\xi_i$.

produce the wake for the ionization of the inner shell electrons. A mixture of preionized plasma and He^{1+} ions is used. The electric field of the electron beam is low enough to not doubly ionize the He. The simulation window has a dimension of $127 \times 127 \times 127\ \mu$m with $1000 \times 1000 \times 5000$ cells in the x, y, and z directions, respectively. An injection laser with the same parameters used above (Fig. 2) is focused into the wake as shown in Fig. 3(a). The laser is focused at $z = 0$ mm while the plasma starts from $z = -0.254$ mm. By tracking particles, we confirm that the trapping condition [4] $\psi_f \approx \psi_i - 1$, as shown in Fig. 3(b). In Fig. 3(c), we present the phase space distribution of the trapped charge after $z = 0.9$ mm for a case where the relative longitudinal position between the beam driver and the injection laser is chosen to achieve $\bar{\xi}_i \approx 1.87$. For this case, based on Eq. (3) the predicted modulator factor is $h \approx 2.9$. The bunching factor $b(k)$ is shown in Fig. 3(b), which is stable when the beam is accelerated from 5.6 to 43.2 MeV. The current profile and the corresponding Wigner transform of the injected charge are shown in Fig. 3(d). The white line $k/k_0 = 2\sqrt{4 + \xi_i^2}/\xi_i$ does not follow within the center of the Wigner transform because the rear of the wake deviates from a sphere [26,27].

By replacing the 800 nm injection laser by its fourth harmonic 200 nm injection laser, an electron bunch with a strong UV frequency modulation is generated. We simulate this using OSIRIS with the external wakefield model described above for the same plasma density. A 200 nm injection laser with $a_0 = 0.023$, $w_0 = 2\ \mu$m is used to release the second electron of He. The current profile and the bunching factor at $z = 1.4$ mm are shown in Fig. 4, respectively, where it is seen that individual electrons are microbunched spatially on a nanoscale. Such a nanobunched structure will give rise to intense CTR [21] at the harmonics of the bunching frequency. The CTR energy generated from a sharp plasma-vacuum boundary generated by the modulation within the shaded wave number (frequency) shown in Fig. 4(b) is about 0.02 nJ [30] (we assume the beam has a mean energy $\bar{\gamma} = 1000$). The radiated spectrum will contain the fundamental and the second harmonic of the nanostructured beam at 65.6 and 32.8 nm, respectively. The detection of this coherent radiation at wavelengths shorter than the ionizing laser wavelength is a good diagnostic of this self-bunching in the wake. Space charge interaction between the injected electrons will blur the modulation at nhk_0 and, thus, reduce the modulation and the bunching factor at nhk_0 which can be seen from the comparison between the dashed line ($n_{He^{1+}} = 3 \times 10^{-5} n_p$) and the solid line ($n_{He^{1+}} = 0.3 n_p$) in Fig. 4(b). The velocity dispersion induced by the energy spread inside a single bunch may destroy nanobunching at low beam energies. For the results shown in Figs. 2–4, the energy of the beam is sufficient to ensure that velocity dispersion is not an issue if the beam is further accelerated by the wake.

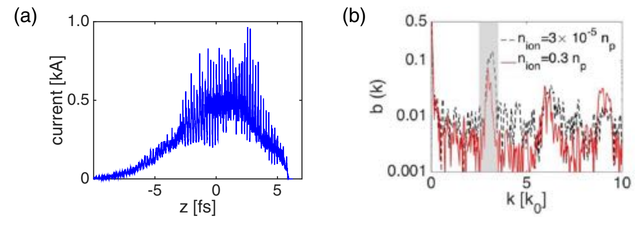

FIG. 4. The current profile (a) and bunching factor (b) of the trapped electrons by using 200 nm injection laser at $z = 1.4$ mm. The red line is the result when $n_{He^{1+}} = 0.3 n_p$, and the black dashed line is the result when $n_{He^{1+}} = 3 \times 10^{-5} n_p$. The energy of the electrons is 50 MeV.

Because of the small spot size and low intensity of the injection laser, the emittance and energy spread of the trapped beam are both very small, e.g., for the 200 nm injection laser case discussed above $\epsilon_{nx,y} = 11$ nm, and uncorrelated energy spread $\sigma_\gamma = 4$. If such an electron beam can be accelerated further while limiting the energy spread extracted from the plasma and coupled into a resonant undulator without degrading its emittance [31], it will produce intense coherent radiation. For example, consider an electron beam with $\bar{\gamma} = 1068.9$ and $\sigma_\gamma = 4$ propagating into a planar undulator with wavelength $\lambda_u = 3$ cm and normalized undulator parameter $K = 2$, which is resonant at the modulation wavelength of the beam,

$\lambda_r = 65.6$ nm. The output radiation power saturates at $P_{\mathrm{sat}} = 140$ MW in a 3.5 m undulator when simulating this process with the GENESIS 1.3 code [32]. As a comparison, another FEL simulation using the same beam parameters except with no initial bunching shows that the radiation power achieves 1.1 MW in a 9 m undulator.

This work was supported by the National Basic Research Program of China Grant No. 2013CBA01501, NSFC Grants No. 11425521, No. 11535006, No. 11375006, and No. 11475101, Thousand Young Talents Program, DOE Grants No. DE-SC0010064, No. DE-SC0014260, and No. DE-SC0008316, and NSF Grants No. ACI-1339893, No. PHY-1415386, and No. PHY-0960344. The simulations were performed on the UCLA Hoffman 2 and Dawson 2 Clusters, and the resources of the National Energy Research Scientific Computing Center and the Blue Waters.

*weilu@tsinghua.edu.cn

[1] C. Joshi and T. Katsouleas, Phys. Today **56**, 47 (2003).
[2] M. Chen, Z.-M. Sheng, Y.-Y. Ma, and J. Zhang, J. Appl. Phys. **99**, 056109 (2006).
[3] E. Oz, S. Deng, T. Katsouleas, P. Muggli, C. D. Barnes, I. Blumenfeld, F. J. Decker, P. Emma, M. J. Hogan, R. Ischebeck *et al.*, Phys. Rev. Lett. **98**, 084801 (2007).
[4] A. Pak, K. A. Marsh, S. F. Martins, W. Lu, W. B. Mori, and C. Joshi, Phys. Rev. Lett. **104**, 025003 (2010).
[5] C. McGuffey, A. G. R. Thomas, W. Schumaker, T. Matsuoka, V. Chvykov, F. J. Dollar, G. Kalintchenko, V. Yanovsky, A. Maksimchuk, K. Krushelnick *et al.*, Phys. Rev. Lett. **104**, 025004 (2010).
[6] C. E. Clayton, J. E. Ralph, F. Albert, R. A. Fonseca, S. H. Glenzer, C. Joshi, W. Lu, K. A. Marsh, S. F. Martins, W. B. Mori *et al.*, Phys. Rev. Lett. **105**, 105003 (2010).
[7] J. S. Liu, C. Q. Xia, W. T. Wang, H. Y. Lu, C. Wang, A. H. Deng, W. T. Li, H. Zhang, X. Y. Liang, Y. X. Leng *et al.*, Phys. Rev. Lett. **107**, 035001 (2011).
[8] B. B. Pollock, C. E. Clayton, J. E. Ralph, F. Albert, A. Davidson, L. Divol, C. Filip, S. H. Glenzer, K. Herpoldt, W. Lu *et al.*, Phys. Rev. Lett. **107**, 045001 (2011).
[9] N. Vafaei-Najafabadi, K. A. Marsh, C. E. Clayton, W. An, W. B. Mori, C. Joshi, W. Lu, E. Adli, S. Corde, M. Litos *et al.*, Phys. Rev. Lett. **112**, 025001 (2014).
[10] B. Hidding, G. Pretzler, J. B. Rosenzweig, T. Königstein, D. Schiller, and D. L. Bruhwiler, Phys. Rev. Lett. **108**, 035001 (2012).
[11] F. Li, J. F. Hua, X. L. Xu, C. J. Zhang, L. X. Yan, Y. C. Du, W. H. Huang, H. B. Chen, C. X. Tang, W. Lu *et al.*, Phys. Rev. Lett. **111**, 015003 (2013).
[12] N. Bourgeois, J. Cowley, and S. M. Hooker, Phys. Rev. Lett. **111**, 155004 (2013).
[13] A. Martinez de la Ossa, J. Grebenyuk, T. Mehrling, L. Schaper, and J. Osterhoff, Phys. Rev. Lett. **111**, 245003 (2013).
[14] L.-L. Yu, E. Esarey, C. B. Schroeder, J.-L. Vay, C. Benedetti, C. G. R. Geddes, M. Chen, and W. P. Leemans, Phys. Rev. Lett. **112**, 125001 (2014).
[15] X. L. Xu, Y. P. Wu, C. J. Zhang, F. Li, Y. Wan, J. F. Hua, C.-H. Pai, W. Lu, P. Yu, C. Joshi *et al.*, Phys. Rev. ST Accel. Beams **17**, 061301 (2014).
[16] X. L. Xu, J. F. Hua, F. Li, C. J. Zhang, L. X. Yan, Y. C. Du, W. H. Huang, H. B. Chen, C. X. Tang, W. Lu *et al.*, Phys. Rev. Lett. **112**, 035003 (2014).
[17] W. P. Leemans, C. E. Clayton, W. B. Mori, K. A. Marsh, A. Dyson, and C. Joshi, Phys. Rev. Lett. **68**, 321 (1992).
[18] W. P. Leemans, C. E. Clayton, W. B. Mori, K. A. Marsh, P. K. Kaw, A. Dyson, C. Joshi, and J. M. Wallace, Phys. Rev. A **46**, 1091 (1992).
[19] A. Lifschitz and V. Malka, New J. Phys. **14**, 053045 (2012).
[20] M. Zeng, M. Chen, L. L. Yu, W. B. Mori, Z. M. Sheng, B. Hidding, D. A. Jaroszynski, and J. Zhang, Phys. Rev. Lett. **114**, 084801 (2015).
[21] W. Leemans, C. Geddes, J. Faure, C. Tóth, J. Van Tilborg, C. Schroeder, E. Esarey, G. Fubiani, D. Auerbach, B. Marcelis *et al.*, Phys. Rev. Lett. **91**, 074802 (2003).
[22] R. A. Fonseca *et al.*, Lect. Notes Comput. Sci. **2331**, 342 (2002).
[23] C. D. Decker and W. B. Mori, Phys. Rev. Lett. **72**, 490 (1994).
[24] M. V. Ammosov, N. B. Delone, and V. P. Krainov, Sov. Phys. JETP **64**, 1191 (1986).
[25] P. Mora and T. M. Antonsen, Jr., Phys. Plasmas **4**, 217 (1997).
[26] W. Lu, C. Huang, M. Zhou, W. B. Mori, and T. Katsouleas, Phys. Rev. Lett. **96**, 165002 (2006).
[27] W. Lu, C. Huang, M. Zhou, M. Tzoufras, F. S. Tsung, W. B. Mori, and T. Katsouleas, Phys. Plasmas **13**, 056709 (2006).
[28] S. Wang, C. E. Clayton, B. E. Blue, E. S. Dodd, K. A. Marsh, W. B. Mori, C. Joshi, S. Lee, P. Muggli, T. Katsouleas *et al.*, Phys. Rev. Lett. **88**, 135004 (2002).
[29] W. B. Mori, IEEE J. Quantum Electron. **33**, 1942 (1997), and references therein.
[30] L. D. Landau, J. Bell, M. Kearsley, L. Pitaevskii, E. Lifshitz, and J. Sykes, *Electrodynamics of Continuous Media*, Vol. 8 (Elsevier, New York, 1984).
[31] X. L. Xu, J. F. Hua, Y. P. Wu, C. J. Zhang, F. Li, Y. Wan, C.-H. Pai, W. Lu, W. An, P. Yu *et al.*, Phys. Rev. Lett. **116**, 124801 (2016).
[32] S. Reiche, Nucl. Instrum. Methods Phys. Res., Sect. A **429**, 243 (1999).